

# Local control for the collective dynamics of self-propelled particles

Everton S. Medeiros and Ulrike Feudel

*Institute for Chemistry and Biology of the Marine Environment,  
Carl von Ossietzky University Oldenburg, 26111 Oldenburg, Germany*

(Dated: May 26, 2023)

Using a paradigmatic model for the motion of interacting self-propelled particles, we demonstrate that local accelerations at the level of individual particles can drive transitions between different collective dynamics. We find that the ability to trigger such transitions is hierarchically distributed among the particles, forming distinctive spatial patterns within the collective. Chaotic dynamics occur during the transitions, which can be attributed to fractal basin boundaries mediating the process. The hierarchical patterns reported here provide decentralized capabilities for controlling artificial swarms.

In nature, groups of self-propelled elements interact and spontaneously form collectives, or swarms, such as flocks of birds [1–3], schools of fish [4], and colonies of bacteria [5, 6]. The functioning of such formations requires a decentralized decision-making process that often relies on pertinent information, e.g., food location, available to only a few constituents [7]. Therefore, a collective decision is based on an efficient transfer of information from local to global scales within these formations [8–11]. The success of such natural mechanisms motivates research toward enabling artificial systems to exhibit similar collective capabilities [12, 13]. To this end, different strategies have been developed [14–21]. However, controlling the switching among different collective patterns via local interventions is an open problem in such applications. A step toward such accomplishment is understanding the boundaries that separate coexisting collective motion (CM).

In this letter, we investigate this issue via computer simulations of a low-density system of interacting self-propelled particles, a suitable model for swarms of artificial elements. As coexistent CMs, we consider two types of behavior exhibited by the particles, a translational and a rotational state. We demonstrate that local accelerations –at the level of individual particles– can trigger transitions between these two collective states. By applying large sets of different accelerations to each particle in a given CM, we observe that the accelerations that trigger transitions form subsets of various sizes, yielding an internal hierarchy among the particles. Remarkably, particles in the upper hierarchy form patterns that remain inalterable for different system sizes and initial conditions. Moreover, we observe chaotic motion during the driven transitions, signaling the presence of fractal boundaries separating the states of CM. Finally, we consider a simplified version of the particle system to demonstrate that homoclinic intersections can generate such fractal basin boundaries.

The equations describing the system with  $N$  interacting particles are given by:

$$\frac{\partial \vec{r}_i}{\partial t} = \vec{v}_i, \quad (1)$$

$$m \frac{\partial \vec{v}_i}{\partial t} = (\alpha - \beta |\vec{v}_i|^2) \vec{v}_i - \vec{\nabla}_i U(\vec{r}_i), \quad (2)$$

where the vectors  $\vec{r}_i$  and  $\vec{v}_i$  are, respectively, the position and velocity of the  $i$ th particle in a plane with  $i = 1, \dots, N$ . The constants  $\alpha$  and  $\beta$  account for a velocity-dependent pumping and dissipation of energy of the system, respectively. The pairwise interaction among the particles is given by the generalized Morse potential:

$$U(\vec{r}_i) = \sum_{j \neq i} \left[ C_r e^{-|\vec{r}_i - \vec{r}_j|/l_r} - C_a e^{-|\vec{r}_i - \vec{r}_j|/l_a} \right], \quad (3)$$

where the parameter pairs  $(C_a, l_a)$  and  $(C_r, l_r)$  specify the respective amplitudes and ranges of the attractive and repulsive terms of the Morse potential. Depending on such interaction parameters, the model in Eqs. (1)-(2) presents qualitatively different CM [22]. We fix  $C_a = 0.5$ ,  $l_a = 2.0$ ,  $C_r = 1.0$ , and  $l_r = 0.5$  corresponding to a regime in which the CM is consistent with swarming [22]. In addition, the applicability of this model has been proved in numerous studies of collective behavior [23–29].

The dynamics of self-propelled particles depends on the interplay of their energy uptake and dissipation [30]. Here, this aspect is captured by the effective friction function (first term in Eq. (2)). This function has a zero at  $\vec{v}_c^2 = \frac{\alpha}{\beta}$ , representing an attractive characteristic velocity that defines two velocity ranges:  $|\vec{v}_i| < |\vec{v}_c|$ , where particles are accelerated, and  $|\vec{v}_i| > |\vec{v}_c|$ , where they are damped [31–33]. Once the velocity  $|\vec{v}_c|$  is established, the effective friction function vanishes, and the system becomes Hamiltonian [22, 31, 32]. However, the particles approach the velocity  $\vec{v}_c$  in two distinct self-organized configurations: i) A rotational state (RS), where the particles rotate around a common center without global translational motion. ii) A translational state (TS), where the particles travel with constant velocity in a crystallized formation. Interestingly, approaching one state or another depends on the system’s initial conditions (ICs), i.e., each state possesses a basin of attraction with respective basin boundaries. Once the ICs are

prescribed, the system goes through a transient phase of motion in which the effective friction is still in action. After approaching one of the states, the particles remain at it with the respective CM, i.e., RS and TS are absorbing states.

We first consider a system with  $N = 3$  particles to capture the essential features of both states. For this case, in the RS, the particles are spatially arranged in a ring rotating with a velocity given by  $|\vec{v}_i| = |\vec{v}_c|$ . The velocity of the center of mass is  $\vec{v}_{cm} = 0$ , see left-hand side of Fig. 1(a). Conversely, in the TS, the particles travel to infinity in a triangle formation with constant individual velocities  $|\vec{v}_i| = |\vec{v}_c|$ , resulting in  $\vec{v}_{cm}^2 = \alpha/\beta$  shown in the left-hand side of Fig. 1(b). We now apply an instantaneous acceleration  $\vec{a}_i$  to one of the particles of each state. This acceleration is prescribed by  $\vec{a}_i = (\Delta v, \theta^\circ)$ , where  $\Delta v$  specifies its amplitude and  $\theta^\circ$  its orientation in a polar diagram centered at the particle velocity  $\vec{v}_i$  right before the acceleration. Following this local action, the system in the RS (TS) undergoes a global transition into TS (RS), Figs. 1(a) and 1(b), respectively. During the transitions to either CM, the particles exhibit a transitory irregular phase of motion; see the middle of Figs. 1(a) and 1(b). Such irregular motion arises from the complexities of the boundaries separating the basins of attraction of these states. In the literature, an irregular transient motion has recently been observed in systems of self-propelled elements [34, 35]. In addition, transitions between RS and TS have been previously observed only in stochastic systems with random noise applied to all system particles [36–38].

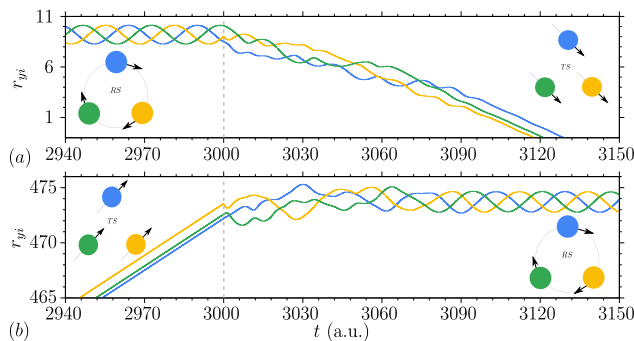


FIG. 1. Time evolution of the system in Eqs. (1)-(2) for  $N = 3$ . An acceleration  $\vec{a}_i$  is applied to one of the particles at  $t = 3000$  (a.u.). (a) For  $\vec{a}_3 = (1.565, 182.43^\circ)$ , a transition is triggered from RS to TS. (b) For  $\vec{a}_3 = (1.361, 191.27^\circ)$ , a transition from TS to RS occurs. Parameters:  $\alpha = 0.15$  and  $\beta = 3.0$ .

Next, we search for sets of local accelerations that can cause collective transitions. First, we define the set  $A_i = \{\vec{a}_i \in \mathbb{R}^2 | \Delta v \in [0, 2], \theta \in [0, 360^\circ]\}$  composed of  $M_i$  applied accelerations equally spaced in this interval. We call  $A_i^{eff}$  the subset of  $A_i$  composed of those accelerations that effectively initiate a transition. In Fig. 2, we show the set  $A_i$  of accelerations  $\vec{a}_i = (\Delta v, \theta)$  applied to the particle  $i = 3$  at  $t = 3000$  (a.u.). The set  $A_3^{eff}$  is

marked in gray. For the system in the RS, we observe that the set  $A_3^{eff}$  of accelerations causing the transition into TS spans an angle  $\theta \approx 180^\circ$  possessing nonsmooth boundaries [Fig. 2(a)]. The minimum amplitude value  $\Delta v$  for the transition is approximately  $2|\vec{v}_c|$ . For the system in the TS, we verify that the set of  $A_3^{eff}$  causing the transition into RS spans an angle  $\theta \approx 120^\circ$  with minimum amplitude  $\Delta v \approx 2|\vec{v}_c|$  also containing nonsmooth boundaries [Fig. 2(b)]. The structure of these boundaries is associated with the irregular motion succeeding the accelerations observed in Fig. 1, i.e., the transition times. To further understand this motion, we show that the probability distribution of their duration  $\tau$  is exponential, an indication of random behavior [Fig 2(c)]. The mean transition time from RS to TS, and vice-versa, is  $\langle \tau \rangle \approx 190$  (a.u.). In addition, we estimate the largest Lyapunov exponents (LLE) corresponding to the transition times. We verify that the average LLE is positive for transitions in both directions and approximately the same ( $\chi_L \approx 0.15$  [Fig. 2(d)], indicating transient chaotic behavior. This chaotic motion points to the existence of an unstable chaotic set (chaotic saddle) embedded in the basin boundaries of the states of CM [39] and mediating the transition in both directions. Chaotic saddles have been identified at the border of a variety of dynamical behaviors [40–47]. The basin boundaries containing embedded chaotic saddles are fractal and are usually extended over large portions of the state space [48, 49]. This feature allows trajectories of individual particles in a given CM to easily access the basins of the opposite state, causing the entire system to switch its collective dynamics.

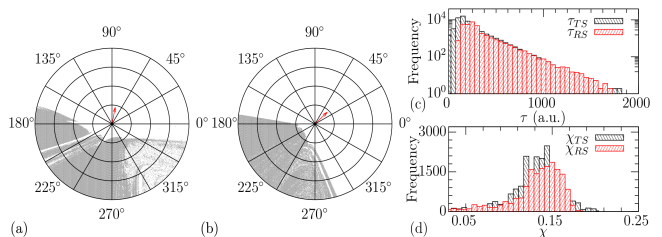


FIG. 2. For  $N = 3$ , polar diagrams  $(\Delta v, \theta)$  illustrating the acceleration set  $A_3$  applied to particle 3 originally in (a) RS and (b) TS. The set of effective accelerations  $A_3^{eff}$  is marked in gray. The red arrow represents the direction of  $\vec{v}$  right before the acceleration is applied. (c) Distribution of transition times  $\tau$  for the system originally in RS (black) and TS (red). (d) LLE  $\chi$  during the transition from RS (black) and from TS (red). Parameters:  $\alpha = 0.15$  and  $\beta = 3.0$ .

We now investigate the set of effective accelerations  $A_i^{eff}$  in more detail. We first show  $A_i^{eff}$  in a polar diagram for accelerations applied at  $t = 1500$  (a.u.) to each particle of a system with  $N = 6$ . For the system initially in the RS (TS), the sets  $A_i^{eff}$  of each particle  $i$  ( $i = 1, \dots, 6$ ) are marked in red [Figs. 3(a)-3(f)] ([Figs. 3(h)-3(n)]). Notice that the size of  $A_i^{eff}$

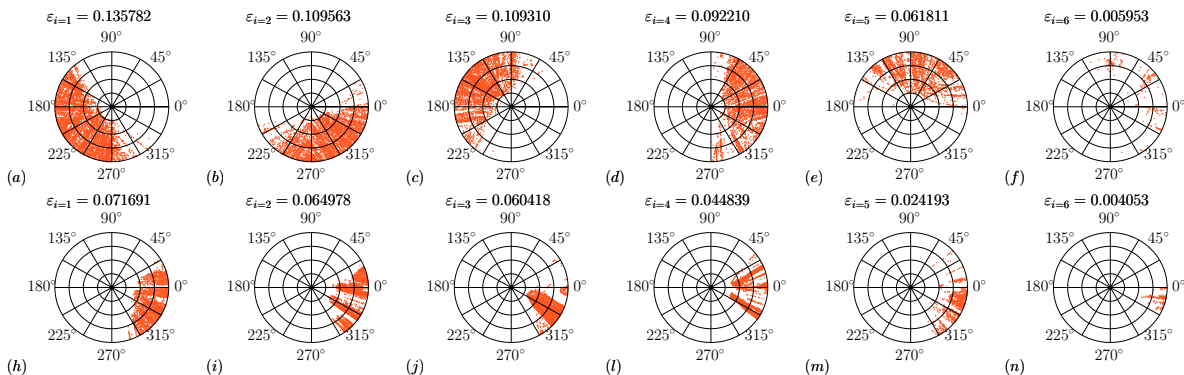


FIG. 3. For the system originally in RS: (a)-(f) Polar diagram ( $\Delta v$ ,  $\theta$ ) of accelerations applied to each particle of the system with  $N = 6$ . (h)-(n) For the system originally in TS. Parameters:  $\alpha = 0.15$  and  $\beta = 3.0$ .

changes among the particles for both CMs. To gain further insights on  $A_i^{eff}$ , we quantify its relative volume as:  $\varepsilon_i = Vol(A_i^{eff} \cap A_i) / Vol(A_i)$ . We estimate this measure by counting the number of effective accelerations

The values of  $\varepsilon_i$  shown in Fig. 3 for both CMs change significantly among the particles, indicating the presence of an internal hierarchy of control effectivity. To validate this possibility, we obtain  $\varepsilon_i$  for particles in different system sizes  $N$  and multiple system realizations with randomly chosen ICs ( $\vec{r}_i(0) \in [0, 2]$  and  $\vec{v}(0) \in [0, 1]$ ). For a given  $N$ , we rank the particles composing the CM in descending order of their  $\varepsilon_i$  values. Subsequently, we average the ordered values of  $\varepsilon_i$  over 7 different sets of ICs to obtain  $\langle \varepsilon_i \rangle$ . Hence, in Fig. 4, we show  $\langle \varepsilon_i \rangle$  (color code) as a function of the particle rank and system size. We verify that  $\langle \varepsilon_i \rangle$  diminishes as the system size increases, reaching the minimum fraction detectable by our estimation,  $1/M_i$ , at  $N = 16$  for the RS [Fig. 4(a)] and  $N = 10$  for the TS [Fig. 4(b)]. The faster diminishing of  $\langle \varepsilon_i \rangle$  indicates that the TS is less susceptible to local accelerations. Moreover, for both CMs, we observe that  $\langle \varepsilon_i \rangle$  decreases monotonically as a function of the rank, demonstrating the hierarchical organizations of the particles within the CMs.

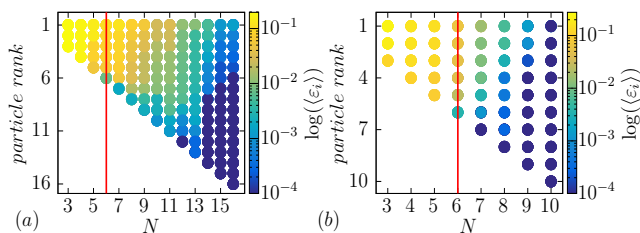


FIG. 4. Average control effectivity  $\langle \varepsilon_i \rangle$  (color code) over 7 different sets of ICs as a function of the particle rank and the system size  $N$ . (a) For the RS. (b) For the TS. The red line indicates the system shown in Fig. 3. Parameters:  $\alpha = 0.15$  and  $\beta = 3.0$ .

$M_i^{eff}$  and dividing it by the total number of accelerations  $M_i = 7895$  applied to each particle  $i$  of a system of size  $N$ . Since  $\varepsilon_i$  accounts for the fraction of effective acceleration of a given particle, it reflects its capability to invoke transitions between the different CM. Therefore, we call  $\varepsilon_i$  control effectivity of a particle  $i$ .

Next, we unravel these hierarchies by investigating the position of the particles with a specific  $\varepsilon_i$  within the CMs at the instant right before the local acceleration. In Fig. 5(a), for the system with  $N = 16$  particles in the RS, we observe that the outer layer of particles possesses the highest values of  $\varepsilon_i$  (color code). For the system with  $N = 8$  in the TS, we observe that particles with the highest  $\varepsilon_i$  occupy the axis transversal to the movement [Fig. 5(e)]. One needs to consider different system ICs and sizes to verify if such observations form statistically significant patterns. In this ensemble approach, the CMs exhibit diverse qualitative features, including different directions of rotation (RS) and translation (TS). To make the realizations comparable, we locate the particles by their position ( $\vec{r}_{xi}$ ,  $\vec{r}_{yi}$ ) related to the system's center of mass [50]. Using these coordinates, we confirm the formation of a clear hierarchical pattern with the particles possessing high  $\varepsilon_i$  in the outer layers of the RS for 7 different sets of ICs [Fig. 5(b)]. To emphasize this pattern for different system sizes, we demonstrate that  $\varepsilon_i$  increases for larger distances to the center of mass  $|\vec{r}_i|$  for  $N = 10$ ,  $N = 13$ , and  $N = 16$  [Fig. 5(c)]. Moreover, we show that the particle's velocity  $|\vec{v}_i|$  averaged over different sizes  $N$  also increases as a function of  $|\vec{r}_i|$  [Fig. 5(d)]. Therefore, unlike the case with  $N = 3$ , the particle velocities are generally not uniform within RS. However, the velocity of particles with high values of  $\varepsilon_i$  (outer layers) approaches the characteristic velocity  $|\vec{v}_c|$  (red line in Fig. 5(d)). For the TS, we confirm that the particles with the highest  $\varepsilon_i$  are distributed along the axis oriented transversally to the direction of motion for 7 different sets of ICs [Fig. 5(f)] [51]. For different  $N$ , we observe that  $\varepsilon_i$  peaks around the angles  $\theta = 0^\circ$  and  $\theta = 180^\circ$  for  $N = 6$ ,  $N = 7$ , and  $N = 8$  [Fig. 5(g)]. The knowledge of such hierarchical patterns within the

states of CM provides a control perspective for artificial swarms.

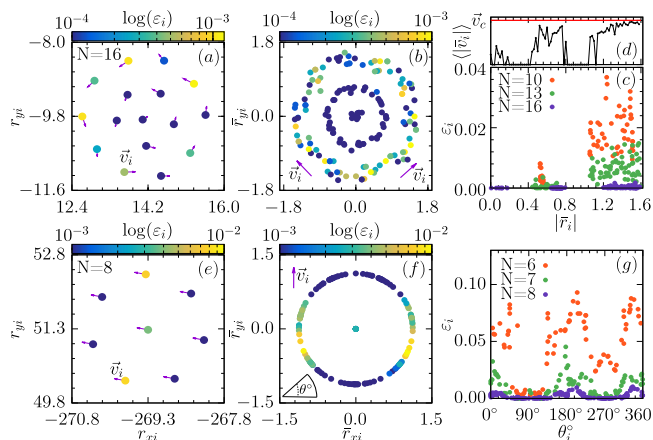


FIG. 5. (a) Pattern of control effectiveness  $\varepsilon_i$  for the RS. (b) 7 realizations of the RS with different ICs. (c) Control effectiveness  $\varepsilon_i$  and (d) averaged velocities  $\langle \bar{v}_i \rangle$  as a function of the distance to the center of mass  $|\bar{r}_i|$  of RS for different  $N$ . (e) Pattern of control effectiveness  $\varepsilon_i$  for the TS. (f) 7 realizations of the TS with different ICs. (g)  $\varepsilon_i$  as a function of  $\theta_i$  for different  $N$ . Parameters:  $\alpha = 0.15$  and  $\beta = 3.0$ .

We show that homoclinic intersections of the stable and unstable manifolds [52, 53] are a mechanism giving rise to such boundaries. We consider a low-dimensional system by perturbing the motion of one particle in a periodically perturbed potential to represent its coupling with other particles. The resulting equation of motion is:

$$\ddot{x} = (\alpha - \beta \dot{x}^2)\dot{x} - \frac{\partial U'(x, t)}{\partial x}, \quad (4)$$

where the interaction is given by  $U'(x) = U(x) + \epsilon x P(t)$  consisting of an one-dimensional Morse potential  $U(x)$  (Eq. (3)) and a periodic forcing  $P(t) = 1 + \sigma \sin(\omega t)$ . The frequency  $\omega = 0.2834$  mimics the oscillations of the other particles, corresponding to the frequency of the particle's oscillations in an unperturbed potential. The parameters  $\epsilon = 0.0088$  and  $\sigma$  control the perturbation's overall amplitude and the periodic forcing's amplitude, respectively. Hence, Eq. (4) yields a three-dimensional state space  $\mathbb{R}^2 \times \mathcal{S}^1$ . Since  $\mathcal{S}^1$  is a periodic component, a stroboscopic mapping is obtained by fixing a cross-section  $\Sigma$  at  $(x, \dot{x}, 0)$ . In Fig. 6, we show the basins of attraction at  $\Sigma$ . White corresponds to ICs converging to the RS, while gray represents the ICs converging to the TS. The boundary between these two basins of attraction is given by the stable manifold  $W_S$  of the saddle point  $x_S^*$ ; (blue curve). The red curve represents the unstable manifold  $W_U$  of  $x_S^*$ . For  $\sigma = 0.01136$ , [Fig. 6(a)], the basin boundary is smooth. The manifolds  $W_S$  and  $W_U$  are close but do not touch each other. For  $\sigma = 0.05682$ , [Fig. 6(b)], the manifolds have intersected at infinitely many points as homoclinic intersections, creating the fractal

basin boundaries. Notice that the fractal basin boundaries occupy a much larger portion of the state space compared to Fig. 6(a). This feature enhances the local control effectivity proposed in this study by increasing the likelihood of accelerations reaching the stable manifold of the saddle point. The manifolds were obtained as in [54].

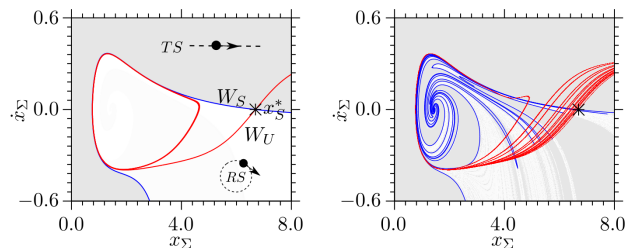


FIG. 6. Basins of attraction at the cross-section  $\Sigma$ . The white color corresponds to RS, while gray to TS. The blue (red) curve is the stable (unstable) manifold of the saddle point  $x_S^*$ . (a) Smooth basin boundaries for  $\sigma = 0.01136$ . (b) Fractal basin boundaries for  $\sigma = 0.05682$ . Parameters:  $\alpha = 0.2$  and  $\beta = 2.0$ .

In summary, we have demonstrated the existence of distinct hierarchical patterns of control effectivity within the spatial organization of two states of CM. These patterns pinpoint the particles in which an applied acceleration has the highest chance of flipping the CM from a rotational to a translational state and vice-versa. For the rotational state, we find that the controllability increases with the distance from the center of rotation. For the translational state, the particles along the axis transversal to the motion are higher in the hierarchy, dictating the control effectivity. These patterns occur for a variety of system sizes and initial conditions. The spatial disposition of these patterns may change for CMs with symmetries and internal velocity profiles not covered here, yet their hierarchical structure is general. Furthermore, we observe chaotic transients during collective state transitions, revealing the existence of fractal sets separating these states. This fractal boundary increases the likelihood of transitions due to its extended coverage of the system state space. In a simplified version of the model, we demonstrate the development of fractal boundaries via homoclinic intersections.

These hierarchical patterns offer a fresh insight into controlling artificial swarms of self-propelled particles in a decentralized manner, i.e., steering the swarm by controlling just one of the self-propelled elements. These findings shall encourage further research on verifying these hierarchies experimentally, examining their scalability in higher-density systems, and exploring their presence in other types of collective behavior.

## ACKNOWLEDGMENTS

E.S.M and U.F. acknowledge the support by the Deutsche Forschungsgemeinschaft (DFG) via the project number 454054251 (FE 359/22-1). The simulations were performed at the HPC Cluster CARL, located at the

University of Oldenburg (Germany) and funded by the DFG through its Major Research Instrumentation Program (INST 184/157-1 FUGG) and the Ministry of Science and Culture (MWK) of the Lower Saxony State, Germany.

- 
- [1] M. Ballerini, N. Cabibbo, R. Candelier, A. Cavagna, E. Cisbani, I. Giardina, A. Orlandi, G. Parisi, A. Procaccini, M. Viale, *et al.*, Empirical investigation of starling flocks: a benchmark study in collective animal behaviour, *Animal Behaviour* **76**, 201 (2008).
- [2] I. L. Bajec and F. H. Heppner, Organized flight in birds, *Animal Behaviour* **78**, 777 (2009).
- [3] D. J. Pearce, A. M. Miller, G. Rowlands, and M. S. Turner, Role of projection in the control of bird flocks, *Proceedings of the National Academy of Sciences* **111**, 10422 (2014).
- [4] B. L. Partridge, The structure and function of fish schools, *Scientific American* **246**, 114 (1982).
- [5] A. Sokolov, I. S. Aranson, J. O. Kessler, and R. E. Goldstein, Concentration dependence of the collective dynamics of swimming bacteria, *Phys. Rev. Lett.* **98**, 158102 (2007).
- [6] D. B. Kearns, A field guide to bacterial swarming motility, *Nature Reviews Microbiology* **8**, 634 (2010).
- [7] S. G. Reeb, Can a minority of informed leaders determine the foraging movements of a fish shoal?, *Animal Behaviour* **59**, 403 (2000).
- [8] I. D. Couzin, J. Krause, N. R. Franks, and S. A. Levin, Effective leadership and decision-making in animal groups on the move, *Nature* **433**, 513 (2005).
- [9] A. Attanasi, A. Cavagna, L. Del Castello, I. Giardina, T. S. Grigera, A. Jelić, S. Melillo, L. Parisi, O. Pohl, E. Shen, *et al.*, Information transfer and behavioural inertia in starling flocks, *Nature physics* **10**, 691 (2014).
- [10] A. Attanasi, A. Cavagna, L. Del Castello, I. Giardina, A. Jelic, S. Melillo, L. Parisi, O. Pohl, E. Shen, and M. Viale, Emergence of collective changes in travel direction of starling flocks from individual birds' fluctuations, *Journal of The Royal Society Interface* **12**, 20150319 (2015).
- [11] A. Ziepke, I. Maryshev, I. S. Aranson, and E. Frey, Multi-scale organization in communicating active matter, *Nature Communications* **13**, 1 (2022).
- [12] M. Brambilla, E. Ferrante, M. Birattari, and M. Dorigo, Swarm robotics: a review from the swarm engineering perspective, *Swarm Intelligence* **7**, 1 (2013).
- [13] M. Schranz, M. Umlauft, M. Sende, and W. Elmenreich, Swarm robotic behaviors and current applications, *Frontiers in Robotics and AI* **7**, 36 (2020).
- [14] O. Soysal and E. Sahin, Probabilistic aggregation strategies in swarm robotic systems, in *Proceedings 2005 IEEE Swarm Intelligence Symposium, 2005. SIS 2005.* (IEEE, 2005) pp. 325–332.
- [15] A. E. Turgut, H. Çelikkanat, F. Gökçe, and E. Şahin, Self-organized flocking in mobile robot swarms, *Swarm Intelligence* **2**, 97 (2008).
- [16] E. Ferrante, A. E. Turgut, C. Huepe, A. Stranieri, C. Pinciroli, and M. Dorigo, Self-organized flocking with a mobile robot swarm: a novel motion control method, *Adaptive Behavior* **20**, 460 (2012).
- [17] G. Francesca, M. Brambilla, A. Brutschy, V. Trianni, and M. Birattari, Automode: A novel approach to the automatic design of control software for robot swarms, *Swarm Intelligence* **8**, 89 (2014).
- [18] A. Cavagna, I. Giardina, T. S. Grigera, A. Jelic, D. Levine, S. Ramaswamy, and M. Viale, Silent flocks: Constraints on signal propagation across biological groups, *Phys. Rev. Lett.* **114**, 218101 (2015).
- [19] G. Vásárhelyi, C. Virágh, G. Somorjai, T. Nepusz, A. E. Eiben, and T. Vicsek, Optimized flocking of autonomous drones in confined environments, *Science Robotics* **3**, eaat3536 (2018).
- [20] Z. Firat, E. Ferrante, Y. Gillet, and E. Tuci, On self-organised aggregation dynamics in swarms of robots with informed robots, *Neural Computing and Applications* **32**, 13825 (2020).
- [21] V. Edwards, P. deZonia, M. A. Hsieh, J. Hindes, I. Triandaf, and I. B. Schwartz, Delay induced swarm pattern bifurcations in mixed reality experiments, *Chaos: An Interdisciplinary Journal of Nonlinear Science* **30**, 073126 (2020).
- [22] M. R. D'Orsogna, Y. L. Chuang, A. L. Bertozzi, and L. S. Chayes, Self-propelled particles with soft-core interactions: Patterns, stability, and collapse, *Phys. Rev. Lett.* **96**, 104302 (2006).
- [23] Y. li Chuang, M. R. D'Orsogna, D. Marthaler, A. L. Bertozzi, and L. S. Chayes, State transitions and the continuum limit for a 2d interacting, self-propelled particle system, *Physica D: Nonlinear Phenomena* **232**, 33 (2007).
- [24] J. Strefler, U. Erdmann, and L. Schimansky-Geier, Swarming in three dimensions, *Phys. Rev. E* **78**, 031927 (2008).
- [25] N. H. Nguyen, E. Jankowski, and S. C. Glotzer, Thermal and athermal three-dimensional swarms of self-propelled particles, *Phys. Rev. E* **86**, 011136 (2012).
- [26] D. Armbruster, S. Martin, and A. Thatcher, Elastic and inelastic collisions of swarms, *Physica D: Nonlinear Phenomena* **344**, 45 (2017).
- [27] J. Hindes, V. Edwards, M. A. Hsieh, and I. B. Schwartz, Critical transition for colliding swarms, *Phys. Rev. E* **103**, 062602 (2021).
- [28] J. Hindes, V. Edwards, K. S. Kasraie, G. Stantchev, and I. B. Schwartz, Swarm shedding in networks of self-propelled agents, *Scientific Reports* **11**, 1 (2021).
- [29] J. Yang, R. Ni, and M. P. Ciamarra, Interplay between jamming and motility-induced phase separation in persistent self-propelling particles, *Phys. Rev. E* **106**, L012601 (2022).
- [30] S. Ramaswamy, Active matter, *Journal of Statistical Mechanics: Theory and Experiment* **2017**, 054002 (2017).
- [31] F. Schweitzer, W. Ebeling, and B. Tilch, Complex mo-

- tion of brownian particles with energy depots, Phys. Rev. Lett. **80**, 5044 (1998).
- [32] W. Ebeling, F. Schweitzer, and B. Tilch, Active brownian particles with energy depots modeling animal mobility, Biosystems **49**, 17 (1999).
- [33] F. Schweitzer, W. Ebeling, and B. Tilch, Statistical mechanics of canonical-dissipative systems and applications to swarm dynamics, Phys. Rev. E **64**, 021110 (2001).
- [34] A. Pikovsky, Transition to synchrony in chiral active particles, Journal of Physics: Complexity **2**, 025009 (2021).
- [35] I. S. Aranson and A. Pikovsky, Confinement and collective escape of active particles, Phys. Rev. Lett. **128**, 108001 (2022).
- [36] A. S. Mikhailov and D. H. Zanette, Noise-induced breakdown of coherent collective motion in swarms, Phys. Rev. E **60**, 4571 (1999).
- [37] U. Erdmann, W. Ebeling, and V. S. Anishchenko, Excitation of rotational modes in two-dimensional systems of driven brownian particles, Phys. Rev. E **65**, 061106 (2002).
- [38] U. Erdmann, W. Ebeling, and A. S. Mikhailov, Noise-induced transition from translational to rotational motion of swarms, Phys. Rev. E **71**, 051904 (2005).
- [39] Y.-C. Lai and T. Tél, *Transient chaos: complex dynamics on finite time scales*, Vol. 173 (Springer Science & Business Media, 2011).
- [40] J. D. Skufca, J. A. Yorke, and B. Eckhardt, Edge of chaos in a parallel shear flow, Phys. Rev. Lett. **96**, 174101 (2006).
- [41] B. Eckhardt, T. M. Schneider, B. Hof, and J. Westerweel, Turbulence transition in pipe flow, Annual review of fluid mechanics **39**, 447 (2007).
- [42] E. L. Rempel and A. C.-L. Chian, Origin of transient and intermittent dynamics in spatiotemporal chaotic systems, Phys. Rev. Lett. **98**, 014101 (2007).
- [43] M. Joglekar, U. Feudel, and J. A. Yorke, Geometry of the edge of chaos in a low-dimensional turbulent shear flow model, Phys. Rev. E **91**, 052903 (2015).
- [44] G. Ansmann, K. Lehnertz, and U. Feudel, Self-induced switchings between multiple space-time patterns on complex networks of excitable units, Phys. Rev. X **6**, 011030 (2016).
- [45] T. Lilienkamp, J. Christoph, and U. Parlitz, Features of chaotic transients in excitable media governed by spiral and scroll waves, Phys. Rev. Lett. **119**, 054101 (2017).
- [46] V. Lucarini and T. Bódai, Transitions across melancholia states in a climate model: Reconciling the deterministic and stochastic points of view, Phys. Rev. Lett. **122**, 158701 (2019).
- [47] E. S. Medeiros, R. O. Medrano-T, I. L. Caldas, and U. Feudel, The impact of chaotic saddles on the synchronization of complex networks of discrete-time units, Journal of Physics: Complexity **2**, 035002 (2021).
- [48] G.-H. Hsu, E. Ott, and C. Grebogi, Strange saddles and the dimensions of their invariant manifolds, Phys. Lett. A **127**, 199 (1988).
- [49] L. Poon and C. Grebogi, Controlling complexity, Phys. Rev. Lett. **75**, 4023 (1995).
- [50] The coordinates of the center of mass are given by  $r_{xcm} = 1/N \sum_i^N r_{xi}$  and  $r_{ycm} = 1/N \sum_i^N r_{yi}$ . Hence, we define the coordinates of the particles with respect to the center of mass as  $\tilde{r}_{xi} = r_{xcm} - r_{xi}$  and  $\tilde{r}_{yi} = r_{ycm} - r_{yi}$ .
- [51] For various ICs in the TS, the system moves in different directions within physical space. To ensure comparability of realizations without affecting the interpretation of results, we rotate the spatial components of the center of mass, causing all realizations to move in the same direction in the diagram depicted in Fig. 5(f).
- [52] S. W. McDonald, C. Grebogi, E. Ott, and J. A. Yorke, Fractal basin boundaries, Physica D: Nonlinear Phenomena **17**, 125 (1985).
- [53] F. C. Moon and G. X. Li, Fractal basin boundaries and homoclinic orbits for periodic motion in a two-well potential, Phys. Rev. Lett. **55**, 1439 (1985).
- [54] D. Ciro, I. L. Caldas, R. L. Viana, and T. E. Evans, Efficient manifolds tracing for planar maps, Chaos: An Interdisciplinary Journal of Nonlinear Science **28**, 093106 (2018).